The growth of ring current/SYM-H under northward IMF B_z conditions present during the 21-22 January 2005 geomagnetic storm

Diptiranjan Rout[1], S. Patra[2], S. Kumar[3], D. Chakrabarty[4], G.D. Reeves[5], C. Stolle[6], K. Pandey[7], S. Chakraborty[8], E. A. Spencer[9]

[1]GFZ German Research Centre for Geosciences, Potsdam, Germany
[2]University of New Brunswick, Canada.
[3]Institute for Space-Earth Environmental Research, Nagoya University, Nagoya, Japan
[4]Physical Research Laboratory, Ahmedabad, India
[5]Los Alamos National Laboratory, Los Alamos, NM, USA
[6]Leibniz Institute of Atmospheric Physics at the University of Rostock Kuhlüngsborn, Germany
[7]ISAS, Department of Physics and Engineering Physics, University of Saskatchewan, Saskatoon, Saskatchewan, Canada
[8]Center for Space Science and Engineering Research Bradley Department of Electrical and Computer Engineering, Virginia Tech, USA
[9]Department of Electrical and Computer Engineering, University of South Alabama

Key Points:

- SYM-H growth under northward IMF conditions and highly stretched magnetotail.
- The central plasma sheet was highly dense during the plateau phase of SYM-H.
- Models need to account for the state of the Magnetosphere to successfully reproduce all the features of the SYM-H index.

Corresponding author: D. Rout, diptiprl89@gmail.com

Abstract

The total energy transfer from the solar wind to the magnetosphere is governed by the reconnection rate at the magnetosphere edges as the IMF B_z turns southward. The delayed response of the ring current to solar wind driving can account for the anomalous growth of the SYM-H under northward IMF B_z. The geomagnetic storm on 21-22 January 2005 is considered to be anomalous as the SYM-H index that signifies the strength of ring current, grows and has a sustained peak value lasting more than 6 hrs under northward IMF B_z conditions. In this work, first the standard WINDMI model is utilized to estimate the growth and decay of various magnetospheric currents by using several solar wind-magnetopsehre coupling functions. However, it is found that the WINDMI model driven by any of these coupling functions is not fully able to explain the enhancement of SYM-H under northward IMF B_z. The SYM-H variations during the entire duration of the storm were only reproduced when the effects of the dense plasma sheet were included in the WINDMI model. The limitations of directly-driven models relying purely on the solar wind parameters and not accounting for the state of the magnetosphere are highlighted by this work.

Plain Language Summary

The energy transfer from the solar wind to the Earth's magnetosphere is most efficient under southward IMF Bz conditions. Generally, the southward IMF Bz drives the ring current which is measured by the Dst/SYM-H index. The storm on 21 January 2005 is one of the rarest events which developed under northward IMF Bz conditions. The geomagnetic disturbances due to the storm, that is signified by the SYM-H index at low latitudes, continued to grow for more than six hours, reaching a minimum value of -101 nT after northward turning of the IMF Bz. In this work, we have tried to estimate the SYM-H by using various solar wind-magnetosphere coupling functions as input to the MINDMI model. However, none of these coupling functions could predict this unusual growth of SYM-H index under the northward IMF Bz conditions. A highly dense plasma sheet was observed during the anomalous period and incorporating this in the WINDMI model led to the successful reproduction of the observed magnetic disturbance. This investigation clearly shows the important role of the state of the magnetosphere in energizing the magnetospheric currents. Therefore, it is suggested that the space weather models need to include both the conditions of solar wind and magnetosphere in order to get a better prediction of the strength of the ring current.

1 Introduction

The energy and mass transfer from the solar wind to the Magnetosphere-Ionosphere(MI) system depends on solar wind parameters and the state of the magnetosphere and ionosphere. A great many theories have been proposed to quantify these interactions (Borovsky, 2013; Newell et al., 2007; Gonzalez, 1990) most of which are based on the classical Dungey paradigm (Dungey, 1961). The largest energy reservoirs in the magnetosphere are the westward flowing ring current and the magnetotail current. The ring current gets energized during a geomagnetic storm when the z-component of Interplanetary magnetic field (IMF B_z) turns southward. The energy transfer from the solar wind is more effective when conditions suitable for magnetic reconnection are present on the dayside magnetopause (Borovsky & Birn, 2014). The orientation of the IMF heavily controls the rate and location of reconnection. While the most effective reconnection happens under southward IMF B_z conditions, other solar wind parameters significantly affect it (Newell et al., 2007).

Magnetospheric dynamics are quite distinct when the IMF B_z is northward. The geoeffectiveness of the solar wind drops significantly under northward IMF conditions. Reconnection takes place at high latitudes leading to a four-cell convection pattern (Burke

et al., 1979). Parameters like the solar wind, IMF B_y, geomagnetic dipole field, and the dipole tilt control the energy and mass transfer during northward IMF (Li et al., 2008; Reistad et al., 2019). Under extended periods of northward IMF B_z conditions the plasma sheet transforms into a cold dense plasma sheet (CDPS) (Sorathia et al., 2019; Taylor et al., 2008). Reconnection occurs at locations poleward of the cusp that lead to the capture of interplanetary flux tubes that sometimes contain filament material by the magnetosphere to create the CDPS (Kozyra et al., 2013; Li et al., 2008; Palmroth et al., 2006). This preconditioning which typically takes about 3 hrs is known to lead to a stronger geomagnetic storm if the IMF B_z turns southward immediately after the period of northward IMF B_z (Wing et al., 2006). The development and recovery of most of the geomagnetic storms in recorded history can be explained by one or more of these simplified theories but there have also been a few reported events that were deemed "anomalous" since the storm was reported to have developed when no energy was being transferred from the solar wind, typically associated with a period of northward IMF B_z (Du et al., 2008; Simi et al., 2012; Kleimenova et al., 2015).

The storm on 21 January 2005 is the only reported event that had a main phase and extended peak lasting more than 6 hrs under northward IMF Bz condition. A few researchers have analyzed the cause of this anomalous storm and modeled it using physics-based and empirical models (Du et al., 2008; Kozyra et al., 2014; Dmitriev et al., 2014; Kalegaev et al., 2015). Storage and delayed injection were provided as a plausible explanation for the enhanced SYM-H during the northward IMF period by Du et al. (2008) and Kane (2012). Others have discussed the unaccounted contributions from additional solar wind parameters, magnetospheric and ionospheric currents (Troshichev & Janzhura, 2012; Dmitriev et al., 2014). The presence of a cold dense plasma sheet that enabled the extreme compression to energize particles adiabatically has also been suggested as a possible energization mechanism (Kozyra et al., 2013). However, none of these theories could properly explain the growth of the ring current under the northward IMF Bz condition. Therefore, the fundamental question that needs to be answered is what drives the ring current during northward IMF Bz conditions when there is no direct energy input from the solar wind. In this study, we successfully reproduce all the features of the 21 January 2005 storm by using the WINDMI model (Horton & Doxas, 1998; Spencer et al., 2007; Patra et al., 2011) driven by a few standard coupling functions to interpret the global magnetosphere-ionosphere system response. The result reveals the strength of the ring current is not only controlled by the solar wind conditions but also depends on the state of magnetosphere.

2 Event Overview

The coronal mass ejection that erupted on 20 January 2005 from the X7.1/3B solar flare in the northwestern quadrant of the solar disk (14°N, 61°W), caused a moderate geomagnetic storm on 21 January 2005 (Foullon et al., 2007). Figure 1 shows the solar wind parameters at the L1 point (in geocentric solar magnetospheric coordinate system) as measured by the Advance Composition Explorer (ACE) satellite. These have been shifted by 24 mins to align with the geomagnetic signatures of the first storm sudden commencement (SSC). The strength of the geomagnetic storm during 21-22 January 2005 as signified by the geomagnetic indices is shown in the figure along with the magnetopause standoff distance (L_{mp} in R_E). This storm is mainly characterized by two storm sudden commencements (indicated as SSC-1 and SSC-2 in red dashed lines) associated with two consecutive interplanetary shocks. The ACE satellite detected a large coronal mass ejection at ∼16:48 UT that arrived at the magnetopause at ∼17:12 UT on 21 January triggering SSC-1 and ∼1.5 hours later (at 18:43 UT) another CME shock front arrived that triggered SSC-2. It can be seen that the solar wind parameters ($|B|$, solar wind density, and velocity) changed sharply at these times. The proton density N increased from 2 cc^{-1} to 22 cc^{-1} during SSC-1 and further increased to an unusually high value

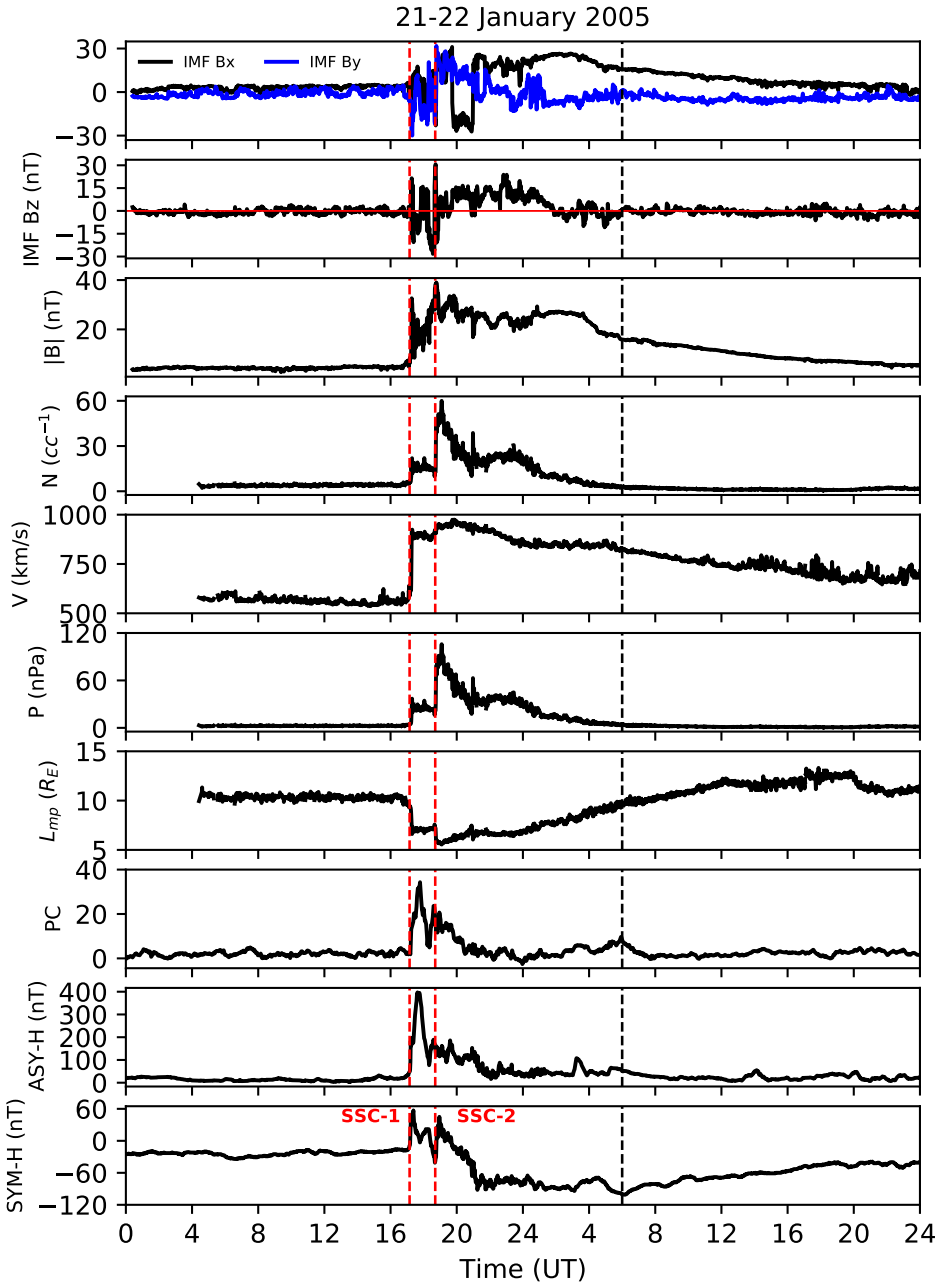

Figure 1. From top to bottom are X and Y components of IMF (IMF B_x and IMF B_y) in blue and black lines, north-south or Z component of IMF (IMF B_z in nT), total magnetic field intensity ($|B|$ in nT), solar wind proton density (N in cc^{-1}), solar wind velocity (V in km/s), solar wind dynamic pressure (P in nPa), variation of the magnetopause standoff distance (L_{mp} in R_E), polar cap index (PC), ASY-H index in nT, and geomagnetic storm index (SYM-H in nT). The red dashed vertical are drawn to identify the SSCs.

of 62 cc^{-1}. The solar wind velocity increased from 565 km/s to 900 km/s. The solar wind dynamic pressure ($P = \frac{1}{2}\rho V^2$) increased from 2 nPa to 35 nPa during the SSC-1 and then it increased to the significantly high value of 106 nPa during SSC-2. Due to the high dynamic pressure, the magnetopause standoff distance was estimated to be significantly reduced from $\sim 10.3\ R_E$ to $5.3\ R_E$ based on the formula provided in Kivelson and Russell (1995). The subsolar magnetopause was continuously located inside geosynchronous orbit ($\sim 6R_E$) due to the strong compression during initial and main phases of the storm. It is for the first time that the upstream solar wind was observed at geosynchronous orbit for almost 2 hr due to the extreme compression caused by the solar wind dynamic pressure (Dmitriev et al., 2014).

In response to SSC-1, the SYM-H increased from -17 nT to 55 nT. Approximately 1.5 hours later (at 18:43 UT) the second shock front arrived causing the SSC-2 that led to a second increase in the SYM-H value. It is around this time that the IMF B_z turned northward, but surprisingly the storm's main phase continued to develop. In between, the IMF B_z turned southward within minutes of the arrival of the SSC-1 at 17:20 UT, it briefly turned northward at 17:47 UT but turned southward again at 18:18 UT, and remained southward until a few minutes before the arrival of the SSC-2 at 18:45 UT. The SYM-H reached it's lowest value of -101 nT at 06:00 UT on 22 January. The IMF B_z was continuously northward from 19:40 UT, 21 January to 02:45 UT, 22 January 2005. Typically, when the IMF B_z turns northward the ring current starts to recover and this recovery is observed in the SYM-H values. But surprisingly during the period from 19:40 UT, 21 January - 02:45 UT, 22 January 2005, the SYM-H index grew to a value of around -90 nT by 21:30 UT and remained elevated afterwards which is referred to as the "plateau" region. This is highly unusual and termed as "anomalous" as reported by a few other studies (Du et al., 2008; McKenna-Lawlor et al., 2010; Kozyra et al., 2013, 2014; Bag et al., 2023). Additionally, the polar cap index (PC), and the indicator of ring current asymmetry (ASY-H) were significantly high during the initial phase but dropped quickly during the main phase.

3 Results and Discussion

In order to explain this unusual growth of the ring current, the low order physics-based model of the magnetosphere-ionosphere system, WINDMI (Horton & Doxas, 1998; Spencer et al., 2007) is used. The WINDMI model is derived from the fluid plasma equations that give a system of eight ordinary differential equations driven by a potential derived from solar wind coupling functions. The eight equations of the model are given by:

$$L\frac{dI}{dt} = V_{\rm sw}(t) - V + M\frac{dI_1}{dt} \quad (1)$$

$$C\frac{dV}{dt} = I - I_1 - I_{\rm ps} - \Sigma V \quad (2)$$

$$\frac{3}{2}\frac{dp}{dt} = \frac{\Sigma V^2}{\Omega_{\rm cps}} - u_0 p K_\parallel^{1/2}\Theta(u) - \frac{pVA_{\rm eff}}{\Omega_{\rm cps}B_{\rm tr}L_y} - \frac{3p}{2\tau_E} \quad (3)$$

$$\frac{dK_\parallel}{dt} = I_{ps}V - \frac{K_\parallel}{\tau_\parallel} \quad (4)$$

$$L_I\frac{dI_1}{dt} = V - V_I + M\frac{dI}{dt} \quad (5)$$

$$C_I\frac{dV_I}{dt} = I_1 - I_2 - \Sigma_I V_I \quad (6)$$

$$L_2\frac{dI_2}{dt} = V_I - (R_{\rm prc} + R_{A2})I_2 \quad (7)$$

$$\frac{dW_{\rm rc}}{dt} = R_{\rm prc}I_2^2 + \frac{pVA_{\rm eff}}{B_{\rm tr}L_y} - \frac{W_{\rm rc}}{\tau_{\rm rc}} \quad (8)$$

The model is driven by a potential field that is a function of the solar wind paramters (V_{sw}) . The nonlinear equations of the model trace the flow of electromagnetic and mechanical energy through eight pairs of transfer terms. The remaining terms describe the loss of energy from the magnetosphere-ionosphere system through plasma injection, ionospheric losses and ring current energy losses. The coefficients in the differential equations are physical parameters of the magnetosphere-ionosphere system. The quantities L, C, Σ, L_1, C_I and Σ_I are the magnetospheric and ionospheric inductances, capacitances, and conductances respectively. A_{eff} is an effective aperture for particle injection into the ring current. The resistances in the partial ring current and region-2 current, I_2 are R_{prc} and R_{A2} respectively, and L_2 is the inductance of the region-2 current. The coefficient u_0 in eqn. 3 is a heat flux limiting parameter. The energy confinement times for the central plasma sheet, parallel kinetic energy and ring current energy are τ_E, τ_k and τ_{rc} respectively. The effective width of the magnetosphere is L_y and the transition region magnetic field is given by B_{tr}. The pressure gradient driven current is given by $I_{ps} = L_x(p/\mu_0)^{1/2}$, where L_x is the effective length of the magnetotail. The outputs of the model relevant to the current study are the magnetotail current (I), ring current energy (W_{rc}), in addition to all the magnetospheric field aligned currents.

The solar wind-magnetosphere interaction is usually quantified by coupling functions. The earliest of these models was the half-wave rectified motional electric field which proposed that the x-component of solar wind velocity (v_x) and the southward component of IMF $B_z(B_s)$ were the most important parameters (Burton et al., 1975). Additional coupling functions have been introduced that account for the effect of dynamic pressure (P), the perpendicular component of the magnetic field (B_T), and the clock angle ($\theta = tan^{-1}(B_y/B_z)$), magnetic flux at the magnetopause (Φ_{mp}), magnetosonic mach number, plasma beta value, mass density of the solar wind upstream of the bow shock (ρ_o), and thermal pressure (P_{th})(Siscoe et al., 2002; Newell et al., 2007; Borovsky, 2008). These coupling functions are combined with the effective thickness of the magnetosphere L_y^{eff} to obtain the driving potential ($V_{sw} = V_{xxx}$) for the model. We have chosen five coupling functions for this study as defined below:

$$V_{rectified} = v_x B_s^{IMF} L_y^{eff} \quad \text{— Rectified} \tag{9}$$

$$V_{siscoe} = 40.0(kV) + 57.6 v_x B_T \sin^2(\theta/2) P^{-1/6} \quad \text{— Siscoe} \tag{10}$$

$$V_{newell} = \frac{d\Phi_{mp}}{dt} = v_x^{4/3} B_T^{2/3} \sin^{8/3}(\theta/2) \quad \text{— Newell} \tag{11}$$

$$V_{newell-P} = P^{1/2} \frac{d\Phi_{mp}}{dt} \quad \text{— Newell-P} \tag{12}$$

$$V_{borovsky} = f(v, B, P, \theta, \rho_o, P_{th}) \quad \text{— Borovsky} \tag{13}$$

For the detailed information of the coupling functions and their performance please refer to Spencer et al. (2011). The chosen coupling functions are normalized based on the method proposed by Spencer et al. (2011), so that only the qualitative differences introduced by each function are highlighted. The WINDMI model estimates the state of the magnetopshere-ionosphere system by optimizing the physical model parameters using a genetic algorithm (Patra et al., 2011). The contribution of the symmetric ring current energy (W_rc) to the SYM-H index is calculated using the Dessler-Parker-Sckopke relationship (Dessler & Parker, 1959; Sckopke, 1966) that relates the energy in the ring current with the magnetic perturbations at low latitudes on the surface of earth. The magnetic perturbation at low latitudes due to the magnetopause currents is estimated as $7.26\sqrt{P}$ based on the empirical relationship given by Burton et al. (1975). The contribution of the tail current (I) to the SYM-H index is estimated from the tail current magnitude calculated by the WINDMI model in eqn. 1 multiplied by a geometric factor (Patra et al., 2011). The sum of all three current contributions gives the estimated

SYM-H value calculated by the WINDMI model for each of the coupling functions as shown in fig 2.

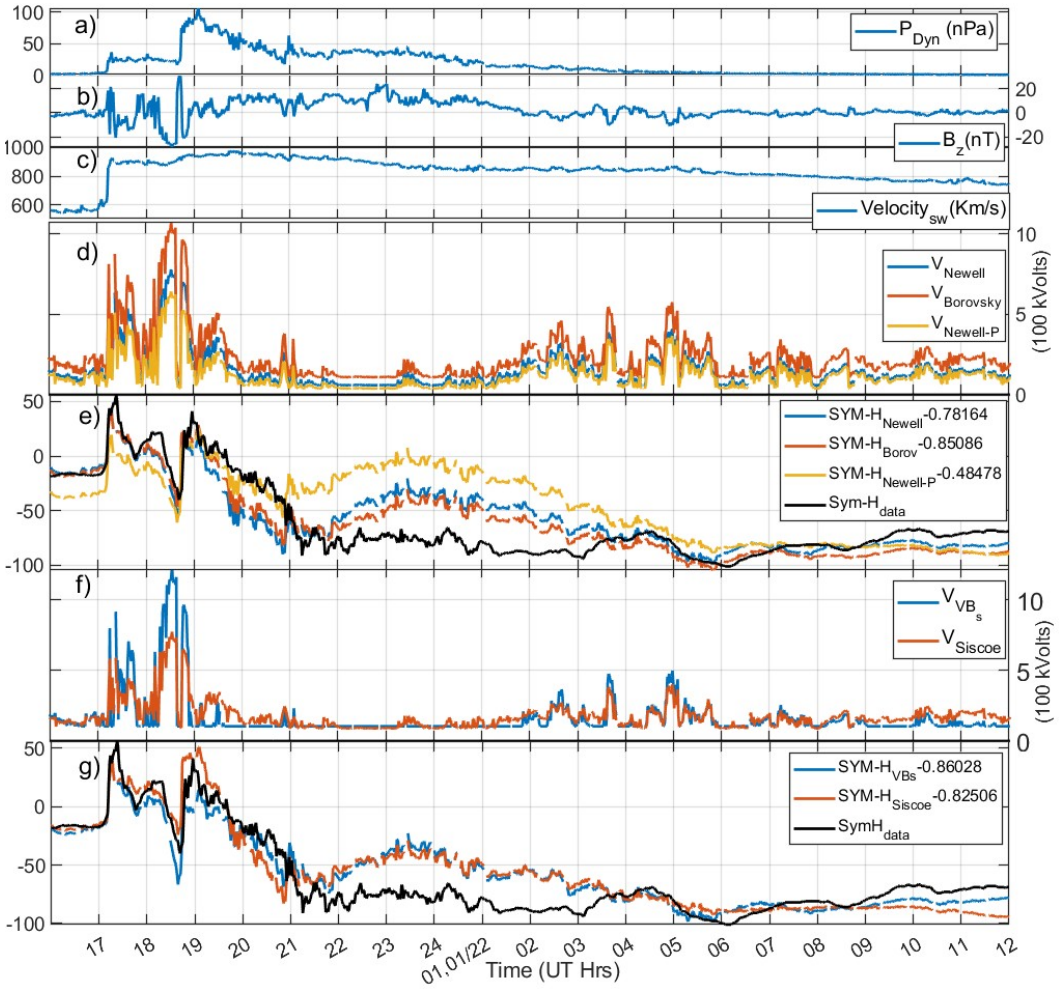

Figure 2. Top three panels (a-c) show the shifted solar wind dynamic pressure, z-component of magnetic field, and velocity measured at ACE. The coupling functions (d,f), the modeled and measured SYM-H values (e,g) along with their correlation coefficients for the 21 January 2005 storm are shown in the bottom four panels.

The best fit results along with the normalized coupling function values are shown in fig. 2 (d-g). During the initial and main phase of the storm until around 21:30 UT, almost all the coupling functions are able to provide acceptable fits. The rectified E-field and Borovsky's coupling functions provide the best fits with correlation values of 0.86 and 0.85 respectively as shown in the panels showing the modeled SYM-H values in fig. 2. The initial growth of the SYM-H after the northward turning of IMF B_z can be correctly estimated due to the reduction in magnetopause currents and the system delay accounted for by the model. From 21:30 UT onwards until 04 UT in the plateau phase the model tends to underpredict the SYM-H values.

The consistent underestimation by the WINDMI model from 21:30 - 04:00 UT is due to the fact that none of the coupling functions predict any substantial energy injection in this period. This suggests that directly driven mechanisms even after account-

ing for other solar wind variables as suggested by Kuznetsova and Laptukhov (2011), and Troshichev and Janzhura (2012), might not have been the dominant contributor to the ring current during this phase. A simple delayed rise of the ring current that can be from 0-8 hrs and slow decay was suggested as a likely cause by Kane (2012), and Gonzalez and Echer (2005). The WINDMI model successfully reproduced the delayed rise in SYM-H, and predicts a slow decay with a relatively high ring current time constant of ~ 40 hrs. The inability of the model to fit the plateau suggests either additional ring current energization mechanisms might have been present or other current sources contributed to the steady SYM-H.

Du et al. (2008) reported that the magnetic field stretching angle was close to zero during the initial phase which signifies a highly distorted magnetosphere and an earthward location of the tail current that suggests a significant contribution from the tail current to the low latitude magnetic disturbance. Empirical and MHD models validated using in-situ and energetic neutral atoms observations have been used to model the various currents' contributions to SYM-H (McKenna-Lawlor et al., 2010; Dmitriev et al., 2014; Kozyra et al., 2014). From these studies, it was inferred that the currents like the field-aligned currents, tail currents, and partial ring current were the dominant contributors during the main and early recovery phase of the storm while the symmetric ring current became dominant after 00:45 UT on 22 January .

Kozyra et al. (2014) reported observations of an intensified auroral oval, isotropic boundary (b2i) at lower latitudes, and the ring current precipitation zones that are evidence for the magnetotail stretching by field line curvature scattering. Kozyra et al. (2013) claim that the 21 January 2005 event was the first and only instance where a strong stretching was observed due to the formation of a dense plasma sheet derived from dense solar filament material. Based on the evidence, it is reasonable to assume that the tail current remained elevated and contributed to the SYM-H index during the main phase. The plasma sheet capacitance parameter C in the WINDMI model eqn. 2 is a function of the plasma sheet density. The capacitance value can be determined using the following expression (Spencer, 2006):

$$C \approx \frac{\pi \rho_m L_x L_z}{B_{x0} B_z L_y} \tag{14}$$

where ρ_m is the plasma sheet density, L_x and L_y are the length and width of the geotail while L_z is the half-width of the plasma sheet. B_{x0} is the magnetic field at $x = 0$ and B_z is constant.

Figure 3(a) shows the plasma sheet density as measured by the Los Alamos National Laboratory Magnetospheric Plasma Analyzers (LANL-MPA). Observations from all the satellites (LANL-95, LANL-84, LANL-97A, LANL-01A, and LANL-02A) during 20:00 - 04:00 magnetic local time (MLT) window are plotted at a given UT. The density increases by almost 6-10 times after the second impulse SSC-2. To reflect this abrupt increase in density we chose a step profile for the plasma sheet capacitance changing from $\sim 70,000F - 560,000F$. The contribution of the various currents to the SYM-H index(SYM-H_{windmi}) as estimated by the WINDMI model driven by the rectified function and density-dependent Capacitance is shown in fig. 3. The model estimates a slow ring current (SYM-H_{rc}) decay with a time constant of ~ 13 hrs. The fast dynamics in the initial and main phases are the result of the Chapman-Ferrao (magnetopause) currents (D_{mp}) and the tail current (SYM-H_{tail}). In the plateau phase the slowly decaying ring current, the still elevated tail current, and the magnetopause current combine to create a near-constant magnetic disturbance that matches with the observed records of the SYM-H index (SYM-H_{data}).

This breakdown of the current contributions to SYM-H also highlights the fallacies in using commonly used terminologies like initial, main, and recovery phases of the

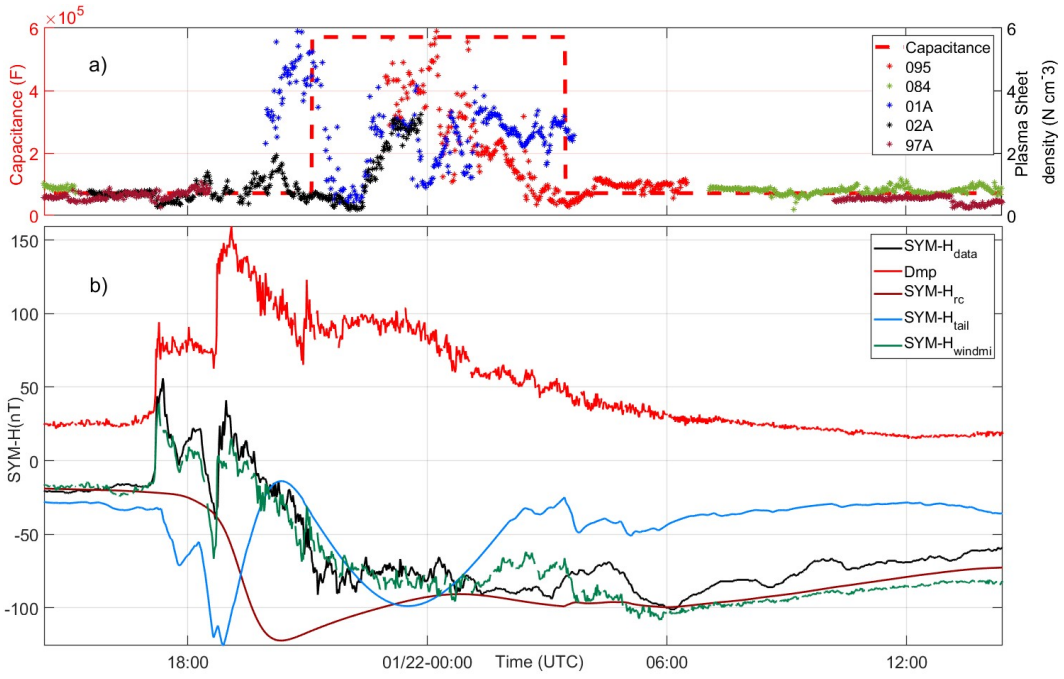

Figure 3. (a) Variation of plasma sheet density measured by different LANL satellites along with the modified plasma sheet capacitance used in the WINDMI model. (b) The best fit currents for the 21 January 2005 storm as estimated by the plasma sheet dependent WINDMI model (see text for details) driven by the rectified VBs input. The magnetopause current (Dmp) is estimated empirically.

storm based on just the SYM-H index. It is clear that the storm's main phase starts much earlier coinciding with the period of negative IMF B_z. The apparent growth of the main phase and the inflection point in SYM-H at 21:15 UT is in fact due to the recovery of the CF-current after the SSC-2 at 19:20 UT. The magnetic perturbation caused by the magnetopause current (D_{mp}) peaked at SSC-2 reaching a value of 55nT and quickly fell down to a value averaging around 80 nT from 21:15 UT till 24 UT. Hence one should be careful in interpreting and trying to model the ring current based purely on the basis of SYM-H.

The occurrence of dense plasma sheet and its role in magnetotail dynamics and ring current intensity was discussed in detail by Borovsky et al. (1997). They suggested three main sources for the higher density: the outer plasmasphere, high density solar wind, and ionospheric outflow. A cold dense plasma sheet usually forms under extended periods of northward IMF B_z (Borovsky & Denton, 2010; Denton & Borovsky, 2012). This dense material can be injected to the inner magnetosphere either by sudden southward IMF or a very strong compression (Thomsen et al., 2003). The long lifetime of the ring current was probably due to particle injection into the inner magnetosphere where the drift times are longer (Dmitriev et al., 2014). The formation of a warm and later cold dense plasma sheet within 1 Hr after impact of the second pressure pulse and under northward IMF conditions was reported by Kozyra et al. (2013) during the 21-22 January 2005 storm. They claim that the high densities were driven by the dense solar filament material that produced strong diamagnetic stretching despite low levels of magnetic activity. Du et al. (2008) suggested that energy was initially stored in the tail due to a previous southward IMF B_z period albeit small and then later injected into the ring current leading to the growth of SYM-H. Although no clear physical mechanism for this was provided, the creation of a dense plasma sheet followed by compression-led injection and substorms could possibly provide the additional source needed.

Fig.4 (left panel) shows the variations of (a) IMF Bz, (b) solar wind pressure (P), electron flux measured at geosynchronous orbit by (c) LANL-1990-095, (d) LANL-01A, (e) LANL-02A satellites and proton flux measured by (f) LANL-01A, (g) LANL-02A satellites (h) the westward auroral electrojet (AL index) during 15:00 UT, 21 Jan-06:00 UT, 22 January. The dashed lines are marked to show the time when dispersionless-like injection of energetic particles at geosynchronous orbit are observed. These satellites were on the night side when the particle enhancements were observed. There are six dispersionless-like injection observed during this event which are also correlated with AL enhancement. It is important to note that three (2nd, 3rd, and 4th) dispersionless-like injection are observed under predominantly northward IMF B_z conditions although the fluxes are relatively low to the quiet time level. It can be seen that the solar wind pressure is high but not changing much during this time. The high solar wind pressure leads to a compressed magnetosphere that can lead to higher losses as the drifting particles might encounter the magnetopause and drift out. Alternatively, the possibility of the LANL satellites to be on higher L-shells can not be ruled out since the magnetosphere is highly stretched. That can also result in lower flux measurements. These substorm-like signatures could then be just signatures of relaxation of the magnetosphere (Kozyra et al., 2013). The presence of a stretched magnetotail sustained by a high tail current and dense plasma sheet during the plateau phase of the storm possibly led to the anomalous SYM-H observations. The counterbalancing contributions from ring current, tail current, magnetopause current and the current wedge formed along with the long lifetimes of the ring current particles during the northward IMF B_z periods might have created conditions for the plateau observed in the SYM-H index (Ohtani et al., 2001; Lopez et al., 2015).

4 Summary

To summarize, in the present investigation, a moderate geomagnetic storm with peak SYM-H value of -110 nT that occurred on 21 January 2005 was unusually found

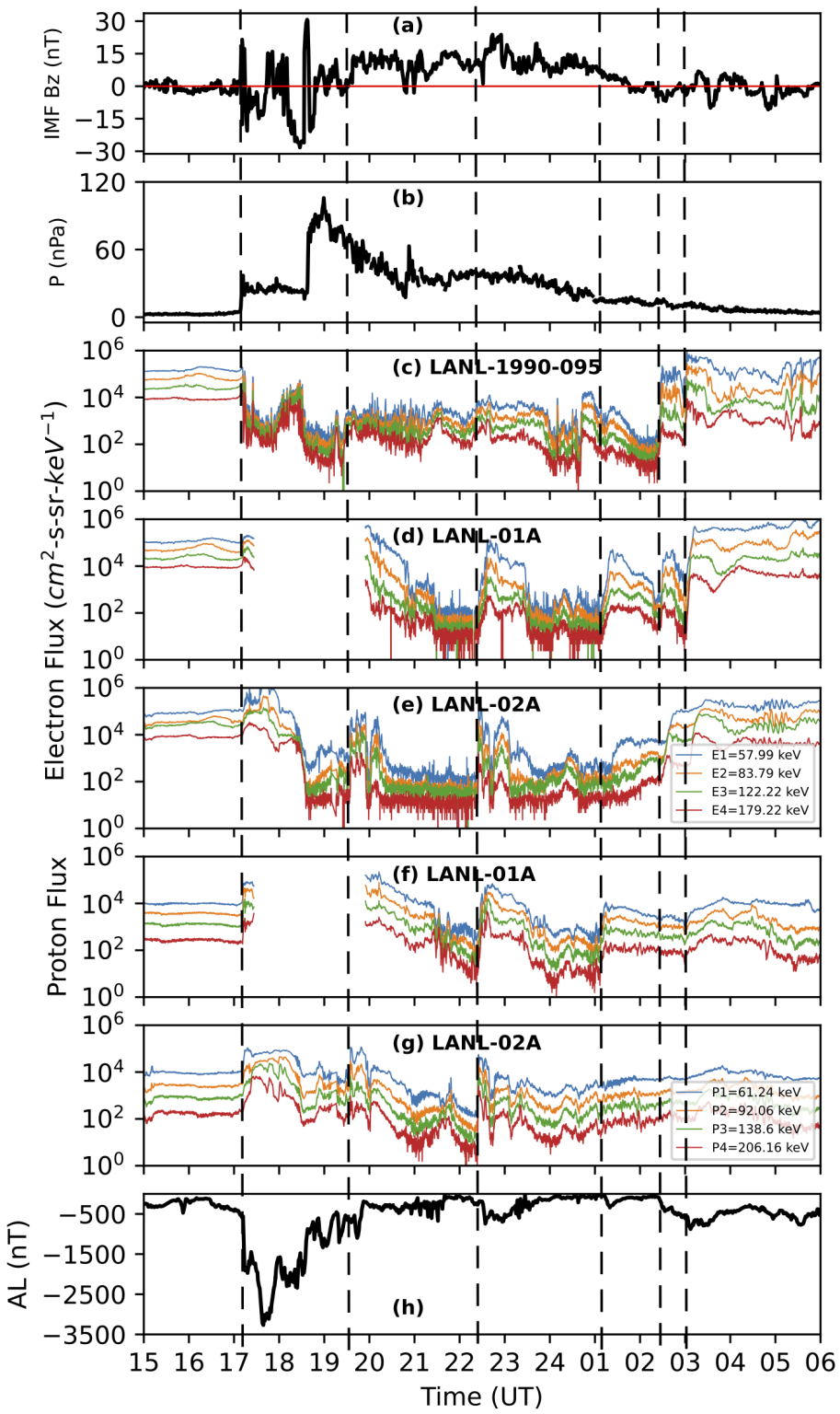

Figure 4. Variations in (a) IMF B_z, (b) Solar wind pressure, electron flux measured at geosynchronous orbit by (c) LANL-1990-095, (d) LANL-01A, (e) LANL-02A satellites, and proton flux measured by (f) LANL-01A, (g) LANL-02A satellites (h) westward auroral electrojet (AL index). The black dashed lines are marked to show the time when the dispersionless-like injections are observed.

to develop under northward IMF B_z conditions. The WINDMI model was used to understand the energization process of the ring current and other currents in the magnetosphere-ionosphere system by considering various coupling functions as input. It is found that the WINDMI fits that used the coupling function of Borovsky and rectified motional electric field as input gave the best correlations with the observed SYM-H. However, it is to be noted that none of the coupling functions could drive currents in the WINDMI model to reproduce the exact variation of SYM-H in the plateau phase. A highly dense plasma sheet was present during the plateau phase of the storm. This coincided with a highly stretched magnetosphere that suggests a sustained high tail current. Multiple "substorm" like signatures were found to be present during the northward IMF B_z conditions in the main phase of the storm that caused magnetic perturbations globally.

The WINDMI model was enhanced to include the contribution of plasma sheet density that allowed the WINDMI model to successfully reproduce all the features of the storm. The model estimates a slowly decaying ring current and a sustained tail current in the plateau phase. The long lifetime of the ring current was probably due to particle injection into the inner magnetosphere where the drift times are longer. A combination of the highly dense plasma sheet, deep injection of the ring current particles, and the elevated levels of the magnetopause currents likely caused the apparent growth, plateau and extremely long recovery of the SYM-H index. The energy transfer from the solar wind to the magnetosphere-ionosphere system is the key to comprehending and predicting space weather. This study highlights the importance of correctly accounting for the state of the magnetosphere in successfully modeling currents during a geomagnetic storm.

5 Open Research-Data availability statement

Data used in this study is made available at `https://zenodo.org/record/7351730#.Y38w7oLMIoJ`. The geomagnetic indices (SYM-H and AL) and solar wind data are obtained from the GSFC/SPDF OMNIWeb (`https://omniweb.gsfc.nasa.gov`). The WINDMI model v.1 can be run for free at the Community coordinated modeling center (CCMC) (`https://ccmc.gsfc.nasa.gov/models/WINDMI~1.0`).

Acknowledgments

D. Rout acknowledges the support from Humboldt research Fellowship for Postdoctoral Researchers (Humboldt foundation grants PSP D-023-20-001).S. Kumar acknowledges the support from Japan Society for the Promotion of Science postdoctoral fellowship (JSPS 22F22329). K. Pandey acknowledges the support of the Canadian Space Agency (CSA), [21SUSTTRRI]. Authors are thankful to acknowledge Los Alamos National Laboratory, New Mexico, USA. for providing the geosynchronous particle injection data.

References

Bag, T., Rout, D., Ogawa, Y., & Singh, V. (2023). Thermospheric no cooling during an unusual geomagnetic storm of 21-22 january 2005: A comparative study between TIMED/SABER measurements and TIEGCM simulations. *Atmosphere*, *14*(3). Retrieved from `https://www.mdpi.com/2073-4433/14/3/556` doi: 10.3390/atmos14030556

Borovsky, J. E. (2008). The rudiments of a theory of solar wind/magnetosphere coupling derived from first principles. *Journal of Geophysical Research: Space Physics*, *113*(A8).

Borovsky, J. E. (2013). Physical improvements to the solar wind reconnection control function for the earth's magnetosphere. *Journal of Geophysical Research: Space Physics*, *118*(5), 2113–2121.

Borovsky, J. E., & Birn, J. (2014). The solar wind electric field does not control

the dayside reconnection rate. *Journal of Geophysical Research: Space Physics*, *119*(2), 751–760.

Borovsky, J. E., & Denton, M. H. (2010). Magnetic field at geosynchronous orbit during high-speed stream-driven storms: Connections to the solar wind, the plasma sheet, and the outer electron radiation belt. *Journal of Geophysical Research: Space Physics*, *115*(A8).

Borovsky, J. E., Thomsen, M. F., & McComas, D. J. (1997). The superdense plasma sheet: Plasmaspheric origin, solar wind origin, or ionospheric origin? *Journal of Geophysical Research: Space Physics*, *102*(A10), 22089–22097.

Burke, W. J., Kelley, M. C., Sagalyn, R. C., Smiddy, M., & Lai, S. T. (1979, January). Polar cap electric field structures with a northward interplanetary magnetic field. *Geophysical Research Letters*, *6*(1), 21-24. doi: 10.1029/GL006i001p00021

Burton, R., McPherron, R., & Russell, C. (1975). An empirical relationship between interplanetary conditions and dst. *Journal of geophysical research*, *80*(31), 4204–4214.

Denton, M., & Borovsky, J. (2012). Magnetosphere response to high-speed solar wind streams: A comparison of weak and strong driving and the importance of extended periods of fast solar wind. *Journal of Geophysical Research: Space Physics*, *117*(A9).

Dessler, A., & Parker, E. N. (1959). Hydromagnetic theory of geomagnetic storms. *Journal of Geophysical Research*, *64*(12), 2239–2252.

Dmitriev, A. V., Suvorova, A. V., Chao, J.-K., Wang, C. B., Rastaetter, L., Panasyuk, M. I., ... Myagkova, I. N. (2014). Anomalous dynamics of the extremely compressed magnetosphere during 21 january 2005 magnetic storm. *Journal of Geophysical Research: Space Physics*, *119*(2), 877-896. Retrieved from `https://agupubs.onlinelibrary.wiley.com/doi/abs/10.1002/2013JA019534` doi: https://doi.org/10.1002/2013JA019534

Du, A., Tsurutani, B., & Sun, W. (2008). Anomalous geomagnetic storm of 21–22 january 2005: A storm main phase during northward imfs. *Journal of Geophysical Research: Space Physics*, *113*(A10).

Dungey, J. W. (1961). Interplanetary magnetic field and the auroral zones. *Physical Review Letters*, *6*(2), 47.

Foullon, C., Owen, C. J., Dasso, S., Green, L. M., Dandouras, I., Elliott, H. A., ... Crooker, N. U. (2007, August). Multi-Spacecraft Study of the 21 January 2005 ICME. Evidence of Current Sheet Substructure Near the Periphery of a Strongly Expanding, Fast Magnetic Cloud. *Solar physics*, *244*(1-2), 139-165. doi: 10.1007/s11207-007-0355-y

Gonzalez, W. (1990). A unified view of solar wind-magnetosphere coupling functions. *Planetary and Space Science*, *38*(5), 627–632.

Gonzalez, W., & Echer, E. (2005). A study on the peak dst and peak negative bz relationship during intense geomagnetic storms. *Geophysical research letters*, *32*(18).

Horton, W., & Doxas, I. (1998). A low-dimensional dynamical model for the solar wind driven geotail-ionosphere system. *Journal of Geophysical Research: Space Physics*, *103*(A3), 4561–4572.

Kalegaev, V., Vlasova, N., & Peng, Z. (2015). Dynamics of the magnetosphere during geomagnetic storms on january 21–22, 2005 and december 14–15, 2006. *Cosmic Research*, *53*(2), 98–110.

Kane, R. (2012). Interplanetary and geomagnetic parameters during january 16–26, 2005. *Planetary and Space Science*, *62*(1), 97–99.

Kivelson, M. G., & Russell, C. T. (1995). *Introduction to Space Physics*.

Kleimenova, N., Gromova, L., Dremukhina, L., Levitin, A., Zelinsky, N., & Gromov, S. (2015). High-latitude geomagnetic effects of the main phase of the geomagnetic storm of november 24, 2001 with the northern direction of imf.

Geomagnetism and Aeronomy, *55*(2), 174–184.

Kozyra, J. U., Liemohn, M. W., Cattell, C., De Zeeuw, D., Escoubet, C. P., Evans, D. S., ... Verkhoglyadova, O. (2014, July). Solar filament impact on 21 January 2005: Geospace consequences. *Journal of Geophysical Research (Space Physics)*, *119*(7), 5401-5448. doi: 10.1002/2013JA019748

Kozyra, J. U., Manchester, W. B., Escoubet, C. P., Lepri, S. T., Liemohn, M. W., Gonzalez, W. D., ... Tsurutani, B. T. (2013, October). Earth's collision with a solar filament on 21 January 2005: Overview. *Journal of Geophysical Research (Space Physics)*, *118*(10), 5967-5978. doi: 10.1002/jgra.50567

Kuznetsova, T., & Laptukhov, A. (2011). Contribution of geometry of interaction between interplanetary and terrestrial magnetic fields into global magnetospheric state and geomagnetic activity. *Advances in space research*, *47*(6), 978–990.

Li, W., Raeder, J., Thomsen, M. F., & Lavraud, B. (2008). Solar wind plasma entry into the magnetosphere under northward imf conditions. *Journal of Geophysical Research: Space Physics*, *113*(A4).

Lopez, R., Gonzalez, W., Vasyliūnas, V., Richardson, I., Cid, C., Echer, E., ... Brandt, P. C. (2015). Decrease in sym-h during a storm main phase without evidence of a ring current injection. *Journal of Atmospheric and Solar-Terrestrial Physics*, *134*, 118–129.

McKenna-Lawlor, S., Li, L., Dandouras, I., Brandt, P. C., Zheng, Y., Barabash, S., ... Strharsky, I. (2010). Moderate geomagnetic storm (21–22 january 2005) triggered by an outstanding coronal mass ejection viewed via energetic neutral atoms. *Journal of Geophysical Research: Space Physics*, *115*(A8). Retrieved from `https://agupubs.onlinelibrary.wiley.com/doi/abs/10.1029/2009JA014663` doi: https://doi.org/10.1029/2009JA014663

Newell, P., Sotirelis, T., Liou, K., Meng, C.-I., & Rich, F. (2007). A nearly universal solar wind-magnetosphere coupling function inferred from 10 magnetospheric state variables. *Journal of Geophysical Research: Space Physics*, *112*(A1).

Ohtani, S., Nosé, M., Rostoker, G., Singer, H., Lui, A., & Nakamura, M. (2001). Storm-substorm relationship: Contribution of the tail current to dst. *Journal of Geophysical Research: Space Physics*, *106*(A10), 21199–21209.

Palmroth, M., Laitinen, T., & Pulkkinen, T. (2006). Magnetopause energy and mass transfer: results from a global mhd simulation. In *Annales geophysicae* (Vol. 24, pp. 3467–3480).

Patra, S., Spencer, E., Horton, W., & Sojka, J. (2011). Study of dst/ring current recovery times using the windmi model. *Journal of Geophysical Research: Space Physics*, *116*(A2).

Reistad, J. P., Laundal, K. M., Østgaard, N., Ohma, A., Thomas, E. G., Haaland, S., ... Milan, S. E. (2019). Separation and quantification of ionospheric convection sources: 2. the dipole tilt angle influence on reverse convection cells during northward imf. *Journal of Geophysical Research: Space Physics*, *124*(7), 6182–6194.

Sckopke, N. (1966). A general relation between the energy of trapped particles and the disturbance field near the earth. *Journal of Geophysical Research*, *71*(13), 3125–3130.

Simi, K., Thampi, S. V., Chakrabarty, D., Pathan, B., Prabhakaran Nayar, S., & Kumar Pant, T. (2012). Extreme changes in the equatorial electrojet under the influence of interplanetary electric field and the associated modification in the low-latitude f region plasma distribution. *Journal of Geophysical Research: Space Physics*, *117*(A3).

Siscoe, G., Erickson, G., Sonnerup, B. Ö., Maynard, N., Schoendorf, J., Siebert, K., ... Wilson, G. (2002). Hill model of transpolar potential saturation: Comparisons with mhd simulations. *Journal of Geophysical Research: Space Physics*, *107*(A6), SMP–8.

Sorathia, K., Merkin, V., Ukhorskiy, A., Allen, R., Nykyri, K., & Wing, S. (2019). Solar wind ion entry into the magnetosphere during northward imf. *Journal of Geophysical Research: Space Physics*, *124*(7), 5461–5481.

Spencer, E. (2006). *Analysis of geomagnetic storms and substorms with the windmi model*. The University of Texas at Austin.

Spencer, E., Horton, W., Mays, M., Doxas, I., & Kozyra, J. (2007). Analysis of the 3–7 october 2000 and 15–24 april 2002 geomagnetic storms with an optimized nonlinear dynamical model. *Journal of Geophysical Research: Space Physics*, *112*(A4).

Spencer, E., Kasturi, P., Patra, S., Horton, W., & Mays, M. (2011). Influence of solar wind–magnetosphere coupling functions on the dst index. *Journal of Geophysical Research: Space Physics*, *116*(A12).

Taylor, M., Lavraud, B., Escoubet, C., Milan, S., Nykyri, K., Dunlop, M., ... others (2008). The plasma sheet and boundary layers under northward imf: A multi-point and multi-instrument perspective. *Advances in Space Research*, *41*(10), 1619–1629.

Thomsen, M., Borovsky, J., Skoug, R., & Smith, C. (2003). Delivery of cold, dense plasma sheet material into the near-earth region. *Journal of Geophysical Research: Space Physics*, *108*(A4).

Troshichev, O., & Janzhura, A. (2012). Magnetic disturbances developing under conditions of northward imf. In *Space weather monitoring by ground-based means* (pp. 219–230). Springer.

Wing, S., Johnson, J. R., & Fujimoto, M. (2006). Timescale for the formation of the cold-dense plasma sheet: A case study. *Geophysical research letters*, *33*(23).

Figure 1.

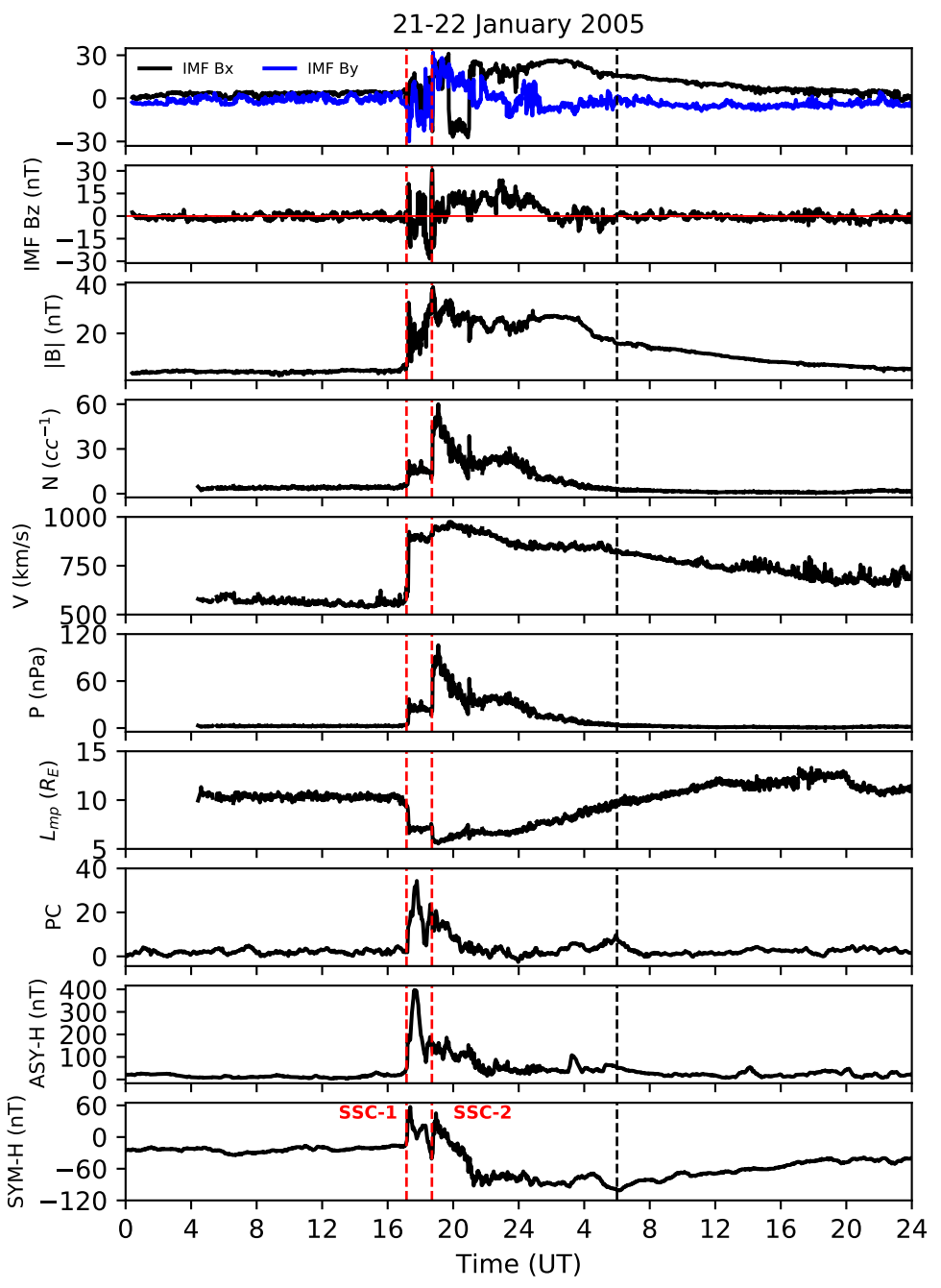
21-22 January 2005
IMF Bx
IMF By
IMF Bz (nT)
|B| (nT)
N (cc^{-1})
V (km/s)
P (nPa)
L_{mp} (R_E)
PC
ASY-H (nT)
SYM-H (nT)
SSC-1
SSC-2
Time (UT)

Figure 2.

a)
b)
c)
d)
e)
f)
g)
P_{Dyn} (nPa)
B_z(nT)
$Velocity_{sw}$(Km/s)
V_{Newell}
$V_{Borovsky}$
$V_{Newell-P}$
(100 kVolts)
$SYM\text{-}H_{Newell}$ -0.78164
$SYM\text{-}H_{Borov}$ -0.85086
$SYM\text{-}H_{Newell-P}$ -0.48478
$Sym\text{-}H_{data}$
V_{VB_s}
V_{Siscoe}
$SYM\text{-}H_{VBs}$ -0.86028
$SYM\text{-}H_{Siscoe}$ -0.82506
$SymH_{data}$
01.01/22
Time (UT Hrs)

Figure 3.

a)

Capacitance (F)

×10^5

Plasma Sheet density (N cm^-3)

Capacitance
095
084
01A
02A
97A

b)

SYM-H(nT)

SYM-H_data
Dmp
SYM-H_rc
SYM-H_tail
SYM-H_windmi

18:00
01/22-00:00
Time (UTC)
06:00
12:00

Figure 4.

(a)
IMF Bz (nT)
30
15
0
−15
−30
(b)
P (nPa)
120
60
0
(c) LANL-1990-095
(d) LANL-01A
(e) LANL-02A
(f) LANL-01A
(g) LANL-02A
Electron Flux (cm^2-s-sr-keV^{-1})
Proton Flux
10^6
10^4
10^2
10^0
E1=57.99 keV
E2=83.79 keV
E3=122.22 keV
E4=179.22 keV
P1=61.24 keV
P2=92.06 keV
P3=138.6 keV
P4=206.16 keV
(h)
AL (nT)
−500
−1500
−2500
−3500
15 16 17 18 19 20 21 22 23 24 01 02 03 04 05 06
Time (UT)